Bulletin of the Seismological Society of America, Vol. 92, No. 5, pp. 1904–1922, June 2002

Integrated Seismic-Hazard Analysis of the Wasatch Front, Utah

by Wu-Lung Chang and Robert B. Smith

Abstract We examined the combined effects of different sources that influence earthquake hazard of the populated Wasatch Front, Utah. We first evaluated the fault-stress interaction of the two largest historic earthquakes of the Intermountain Seismic Belt (ISB): the 1959 Hebgen Lake, Montana (M_s 7.5) and the 1983 Borah Peak, Idaho (M_s 7.3) earthquakes, which experienced multisegment, normal-faulting ruptures. Estimates of the static-stress change for these events revealed an increase in Coulomb failure stress in areas of extended aftershocks. These observations suggested that fault-stress analysis is applicable in evaluating the spatial distribution of aftershocks after large, normal-faulting earthquakes in the same extensional-stress regime of the eastern Basin–Range, including the Wasatch Front, Utah, which encompasses the 370-km-long Wasatch Fault and surrounding faults. On the basis of this result, we applied the modeling technique to the historically seismically quiescent Wasatch Fault and examined the relation between the pattern of stress change and the space–time distribution of paleoearthquakes. Ages and locations of the Wasatch Fault paleoseismic data imply 17 single-segment or 11 multisegment ruptures in the past 5.6 kyr. We prefer the multisegment model because almost all of the large, historical, normal-faulting earthquakes in the ISB were multisegment. Fitting the along-fault displacements by an analytic half-ellipse function provides a first-order distribution of the displacement over an entire rupture length and allows new estimates of fault slip rates and seismic moment. With these data, we also estimated the occurrence rate of $M_w > 6.6$ Wasatch paleoearthquakes and showed that the rate was about three times higher than that inferred by the historical seismicity. This result, along with new information from a "megatrench" on the Wasatch Fault near Salt Lake City, that revealed no scarp-forming earthquakes between ca. 9.0 and 15.5 ka, suggests that large Wasatch Fault events in the past 5.6 kyr may be clustered. The recurrence rate of large earthquakes estimated by the geodetic-measured strain, on the other hand, is three to four times higher than that estimated by the long-term fault-slip rate. This difference, together with the observation of a low regional strain rate from historical seismicity, suggests that cumulative, aseismic deformation may be significant on the Wasatch Fault. We also examined a major consideration for along-strike segmentation, namely, how stress "contagion" could affect the probability of failure of adjacent faults. Including paleoearthquake-derived fault-slip rates, global positioning system derived geodetic moment rates, and the effect of stress contagion in the earthquake-hazard estimation for a specific location in the Salt Lake Valley revealed an increase in the annual frequency of peak ground acceleration $\geq 0.25g$ by a factor of 1.4, 4.0, and 5.4, respectively, compared with that derived from historical seismicity only.

Introduction

The Intermountain Seismic Belt (ISB) is a prominent, north–south-trending zone of earthquakes within the western United States interior that marks an intraplate extensional regime extending 1,300 km from Montana to northern Arizona (Smith and Sbar, 1974; Smith and Arabasz, 1991). In spite of its abundant late-Quaternary and Holocene fault scarps, however, only three scarp-faulting earthquakes have occurred in historical time (Fig. 1): (1) the 1934 $M_s \sim 6.6$ Hansel Valley earthquake on the Hansel Valley Fault, Utah, with a 9-km rupture with ~0.5 m of displacement; (2) the 1959 M_s 7.5 Hebgen Lake earthquake on the Hebgen Lake Fault, Montana, with a 38-km multisegment rupture and up

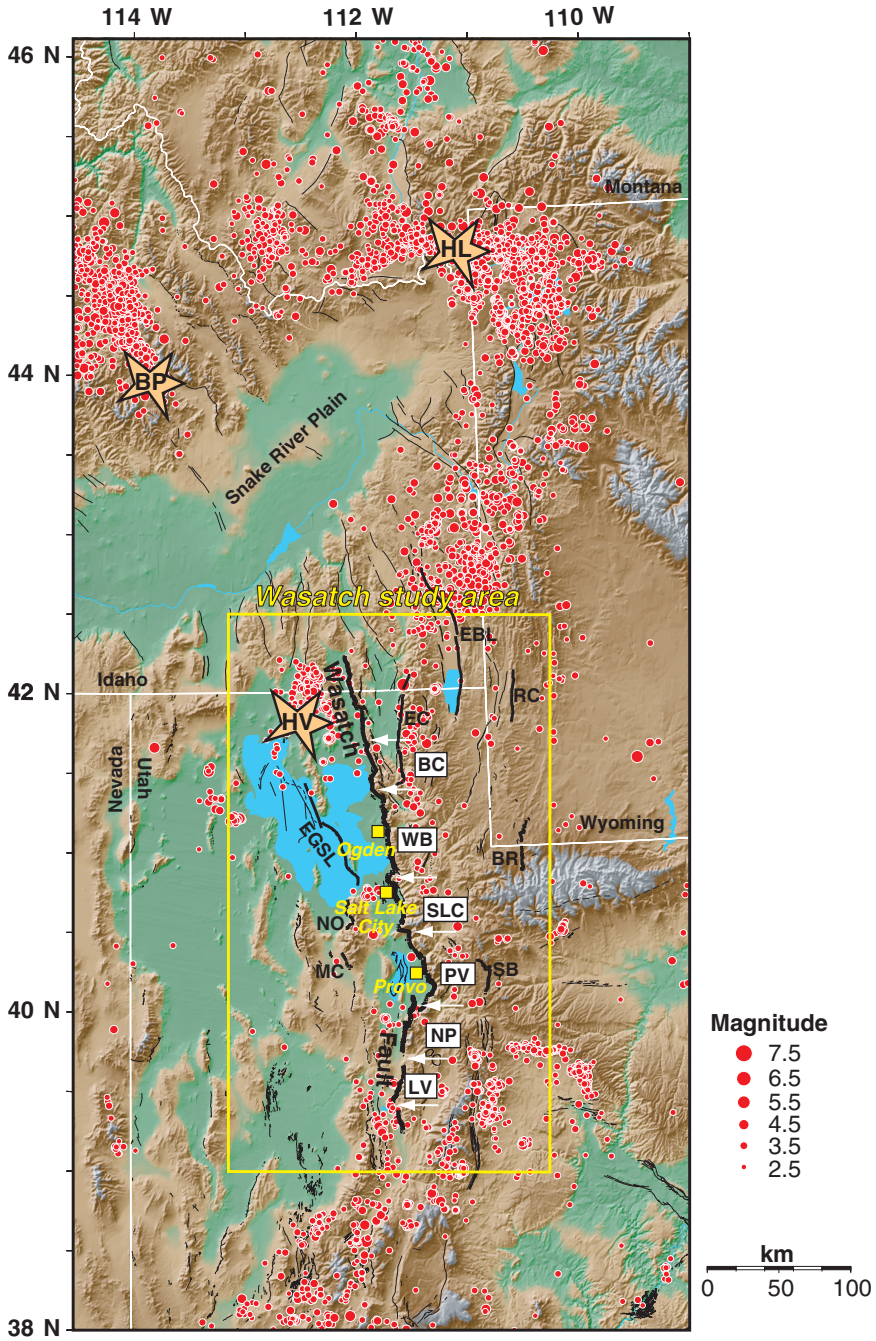

Figure 1. Earthquakes of the central and southern ISB (1962–1996). Three historical surface-faulting earthquakes are shown: HV, M_s 6.6, 1934 Hansel Valley, Utah; HL, M_s 7.5, 1959 Hebgen Lake, Montana; BP, M_s 7.3, 1983 Borah Peak, Idaho. Yellow rectangles indicate cities in the Wasatch Front, Utah, study area (yellow box). Thin, black lines mark late-Quaternary faults, and thick, black lines highlight those studied in this article. The six Holocene-active segments of the Wasatch fault are: BC, Brigham City; WB, Weber; SLC, Salt Lake City; PV, Provo; NP, Nephi; and LV, Levan; other studied faults are (from north to south): EBL, East Bear Lake Fault; RC, Rock Creek Fault; HV, Hansel Valley Fault; EC, East Cache Fault; EGSL, East Great Salt Lake Fault; BR, Bear River Fault; NO, North Oquirrh Fault; MC, Mercur fault; and SB, Strawberry Fault. Earthquake data from compilations of the University of Utah Seismograph Stations for the southern intermountain region and the Idaho National Engineering and Environmental Laboratory by URS Griener Consultants for the central and northern intermountain region (Wong, personnel communication, 1999).

to 6.1 m of displacement; and (3) the 1983 M_s 7.3 Borah Peak earthquake on the Lost River Fault, Idaho, with a 36-km multisegment rupture and a maximum displacement of 2.7 m (Smith and Arabasz, 1991).

Within the central ISB, the 370-km-long Wasatch Fault extends along the west side of the Wasatch Range and traverses the populated Wasatch Front area of Utah, where more than 80% of Utah's 2-million population reside in Salt Lake City, Ogden, and Provo (Fig. 1). On the basis of previous earthquake-hazard studies, the Wasatch Fault has been characterized by six to 10 independent segments, with the youngest surface rupturing about 600 years ago on the Provo segment (e.g., Machette *et al.*, 1992; Hecker, 1993; McCalpin and Nishenko, 1996). In a thorough analysis of the ages of its paleoearthquakes, McCalpin and Nishenko (1996) suggested an average recurrence interval of 350 years for $M > 7$ earthquakes on the fault in the past 5.6 kyr and emphasized that it is the most important source of seismic hazard to this populated area.

The most recent paleoearthquake investigation (McCalpin and Nelson, 2001) on the Wasatch Fault near Salt Lake City focused on extending the time window farther

back than the oldest data from the traditional trenching of 5.6 ka by excavating a 26-m-deep trench called a "mega-trench." This new study revealed an unexpected result, namely, of an extended period of fault quiescence from 9.0 ka to 15.5 ka. This period also corresponds to the unloading of the hanging wall during the desiccation of Quaternary Lake Bonneville, where the lake level reached its highest, 5,090 feet, about 15.5 ka ago and dropped down to 4,250 feet about 9 ka. McCalpin and Nelson (2001) suggested that the earthquakes in the past 5.6 kyr could reflect temporal clustering or that fault-stress loading may have returned to that of the long-term regional Quaternary intraplate-extension rate characteristic of the eastern Basin–Range during the last 10 kyr.

In this study, we first evaluated the methodology of static-stress change to explore how large, normal-faulting earthquakes may affect aftershock distributions and background seismicity. We examined the stress change associated with the 1959 Hebgen Lake and 1983 Borah Peak earthquakes, the two large, historical, ISB normal-faulting earthquakes that notably ruptured more than one segment (Doser, 1985; Barrientos *et al.*, 1987; Crone *et al.*, 1987; Richins *et al.*, 1987). Our results show an excellent correlation between the distributions of static-stress changes and aftershocks for both events, which encourage us to apply the same analysis to the Wasatch and its surrounding faults.

On the basis of the time–space distribution of Wasatch Fault paleoearthquakes, we propose a scenario of multisegment rupturing and estimate fault-slip rates associated with it. We also introduce the effect of stress "contagion" on the calculation of the change of earthquake probability on Wasatch Fault segments. As an example of the integrated analysis, we combined historical seismicity, geological fault-slip rate, geodetic strain rate, and stress contagion to estimate earthquake ground-shaking hazard for a location in the Salt Lake Valley, Utah.

Static-Stress Modeling of Large ISB Earthquakes

Static-stress change is often cited as evidence for systematic space–time variations in aftershock distributions and background seismicity (e.g., Dieterich, 1994; King *et al.*, 1994; Simpson and Reasenberg, 1994; Stein *et al.*, 1997; Harris, 1998; Harris and Simpson, 1998). Rupture perturbs the failure stress of neighboring faults that in turn "encourages" or "suppresses" earthquakes on adjacent faults, depending on the increase or decrease of stress. Our study employed a three-dimensional, elastic boundary-element technique (Simpson and Reasenberg, 1994) to calculate the induced Coulomb failure stress (CFS) on fault planes caused by scenario earthquakes.

M_s 7.5, 1959 Hebgen Lake, Montana, Earthquake

Moment-tensor inversion and modeling of leveling data for the 18 August 1959 Hebgen Lake, Montana, earthquake indicated that two segments of the Hebgen Lake Fault zone, the Hebgen Lake and Red Canyon segments, ruptured during the mainshock (Doser, 1985; Barrientos *et al.*, 1987; Wheeler and Krystinik, 1992). The model that best fits the leveling data revealed that (1) the Red Canyon segment rupture was 18 km long and 12 km wide, with a 45° SW dip and 7.8 m of normal-fault slip and (2) the Hebgen Lake segment rupture was 18 km long and 15 km wide, and had a 50° SW dip with 7.0 m of normal-fault slip (Fig. 2a in Barrientos *et al.*, 1987). We assumed that the regional stress for these areas was uniaxial, N–S extension with a magnitude of 150 bars, based on stress-field inversion of focal mechanisms (Waite and Smith, 2000) and global positioning system (GPS) surveys (Meertens *et al.*, 2000). This value is compatible with the unusually high static-stress drop of about 120 bars observed for the Hebgen Lake mainshock (Doser, 1985).

We estimated the change of the CFS (ΔCFS) on optimal rupture planes at 10-km depth, where these planes are assumed most likely to be ruptured under the regional stress field (N–S extension and 150 bars). We also applied the dry, or drained, model (Simpson and Reasenberg, 1994) by assuming a coefficient of friction of 0.6, and ignored the change in pore pressure because information on rock porosity is unknown for the Wasatch Fault zone. Figure 2a shows that most of the 1959–1975 aftershocks ($M \geq 3$) occurred in the lobes of increased failure stress. Moreover, epicenters of the 1976–1995 extended aftershocks (black circles in Fig. 2a) were also located in the areas of increased failure stress induced by the 1959 mainshock. These results demonstrate a strong spatial correlation between failure–stress change and aftershock distribution.

M_s 7.3, 1983 Borah Peak, Idaho, Earthquake

The 1983 Borah Peak earthquake nucleated about 10 km southwest of the surface rupture of the Thousand Springs segment of the Lost River Fault (Fig. 2b) at a depth of 16 km (Crone *et al.*, 1987; Doser and Smith, 1985). During the mainshock, unilateral rupture propagated northwest along the Thousand Springs segment, passed through a segment boundary, and discontinuously broke both the Thousand Springs and Warm Spring segments (Fig. 2b; Crone *et al.*, 1987; Wheeler and Krystinik, 1992). On the basis of the geometry of mapped fault scarps and geodetic leveling data, Barrientos *et al.* (1987) determined that the rupture of the Thousand Springs segment was 18 km long and 18 km wide and had a 49° SW dip and 2.1 m of slip. The Warm Spring segment, on the other hand, had the corresponding values of 8 km, 8 km, 49° SW, and 1.4 m. Moreover, focal mechanisms of 47 aftershocks indicated that the average regional stress tends to be extensional with a direction of NNE–SSW (Richins *et al.*, 1987). Here we assumed the regional stress of the Borah Peak area to be 100 bars, N30° E uniaxial tension, based on the stress field implied by the aftershocks. We also applied the dry/drained model used in the previous Hebgen Lake model.

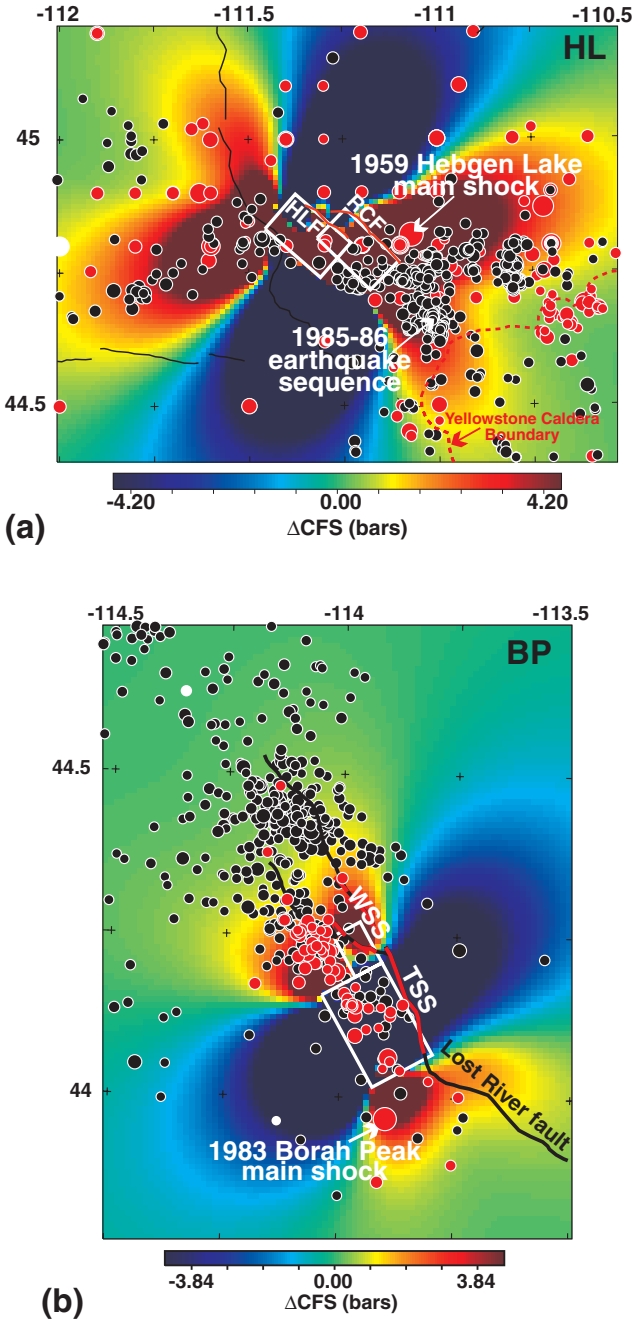

Figure 2. (a) Changes of failure stress at 10-km depth induced by the 1959 Hebgen Lake earthquake (HL), with assumed N–S extensional regional stress of 150 bars. Two fault scarps were formed during the main shock: HLF, the Hebgen Lake Fault, and RCF, the Red Canyon Fault. White boxes show the surface projections of fault planes used for the stress modeling. Circles with different colors show epicenters of aftershocks with magnitude larger than 3.0 in different time periods: white, before the mainshock on 18/08/59; red, 18/08/59–31/12/75; and black, 01/01/76–29/12/95, which include an intense 1985–1986 Yellowstone earthquake sequence. (b) Changes of failure stress at 10-km depth induced by the 1983 Borah Peak earthquake (BP). The main shock ruptured the Thousand Springs (TSS) and the Warm Spring (WSS) segments of the Lost River Fault (black lines). Red lines show the fault scarps, and white rectangles represent the surface projections of the fault planes. Circles with different colors show epicenters of earthquakes with magnitudes larger than 3.0 in different time periods. White circles show foreshocks (01/01/83 to 27/10/83), whereas red and black circles represent earthquakes from 28/10/83 to 18/11/83 (22 days after the mainshock) and 19/11/83 to 29/12/95, respectively. In both figures, areas with warm (red–yellow) colors experienced increasing failure stress, $\Delta CFS > 0$, which means that the occurrence of aftershocks is encouraged on the optimal planes. Areas with blue–green (cold) colors where failure stress decreased, on the other hand, undergo aftershock suppression.

Figure 2b shows the epicenters of Borah Peak aftershocks (1983–1995) together with the failure–stress change at 10-km depth, at which most of the aftershocks were initiated (Richins *et al.*, 1987). The stress changes were estimated for fault planes that have the same geometry as the Lost River Fault (striking N30° W and dipping 49° SW). In Figure 2b, the extended aftershocks migrated northwest into areas that had very low historical seismicity (Richins *et al.*, 1987), and the locations of these aftershocks correlate well with areas experiencing stress increases from a few bars to a few tenths of bars. This result agrees with a conclusion from some other studies that a statio-stress change as low as 0.1 bar can trigger aftershocks (Reasenberg and Simpson, 1992; Hardebeck *et al.*, 1998).

The aforementioned models suggest that the failure–stress change is a good indicator of the spatial distribution of aftershocks for large, normal-faulting earthquakes in the extensional stress regime of the ISB. In addition, studies on western Basin–Range earthquakes have shown similar results. For example, static-stress models of the 1954 Rainbow Mountain (M_s 6.2 and 6.5)–Fairview Peak (M_s 7.2)–Dixie Valley (M_s 6.8) earthquake sequence in central Nevada (Hodgkinson *et al.*, 1996; Caskey and Wesnousky, 1997) revealed that each of these shocks sequentially induced a

stress increase on adjacent faults that failed progressively in time. These results encouraged us to use the same technique to analyze the Wasatch Fault that has not experienced large earthquakes in historical time.

Static-Stress Modeling of Wasatch Fault Earthquakes

Various studies have developed working models for scenario Wasatch Fault earthquakes. For example, on the basis of large, historical, Basin–Range normal-faulting events (see the previous section), we assumed a working model wherein an earthquake occurs on a 45°- to 60°-dipping fault plane and nucleates at 15 to 20 km deep, near the brittle–ductile transition zone (e.g., Smith and Bruhn, 1984; Doser and Smith, 1989; Smith and Arabasz, 1991; Bruhn and Schultz, 1996). From these observations and for the purpose of analytic stress modeling, the Wasatch and nearby faults were discretized into rectangular patches ~10 km long, dipping 55° W, and extending from the surface to 15 km deep (Fig. 3a) with rake angles of −90° (pure normal fault). We also assumed a regional stress of 100 bars and E–W extension for the area, based on studies of focal mechanisms (Zoback, 1989).

In the next section, we will first describe the segmentation of the Wasatch Fault, although large, historical ISB earthquakes, like the Hebgen Lake and Borah Peak events, have ruptured more than one segment. We will then elaborate on how the elastic dislocation method is applied to model the failure–stress change on nearby fault segments. The effect of stress loading or relaxation on faults will be considered as an input to the earthquake-probability estimation, which will be discussed later in this article.

Fault Segmentation

Swan *et al.* (1980) first proposed that rupture on the Wasatch Fault was proportioned among segments: parts of the fault tend to rupture independently of one another during large earthquakes. They suggested six segments on the basis of homogeneous fault properties and historical seismicity and as many as 10 segments based on the geometric change along the fault. Schwartz and Coppersmith (1984), moreover, defined the widely held concept of the "characteristic" earthquake model, in which "seismic-energy release on a given segment occurs mostly as earthquakes of a size that is characteristic of the segment." The assumption was thus that characteristic earthquakes would rupture an entire segment but would not rupture onto adjacent segments. Both studies introduced the concept that ruptures of the Wasatch Fault were confined to discrete segments.

Various factors could control the location and length of rupture. For example, King and Nábelek (1985) proposed that rupture could be limited to regions between bends in faults and terminated at geometric barriers defined as conservative or nonconservative, depending on the shape of the barrier. To test the segmentation hypothesis for the Wasatch Fault, Wheeler and Krystinik (1992) examined several types of information that included gravity anomalies, earthquake-

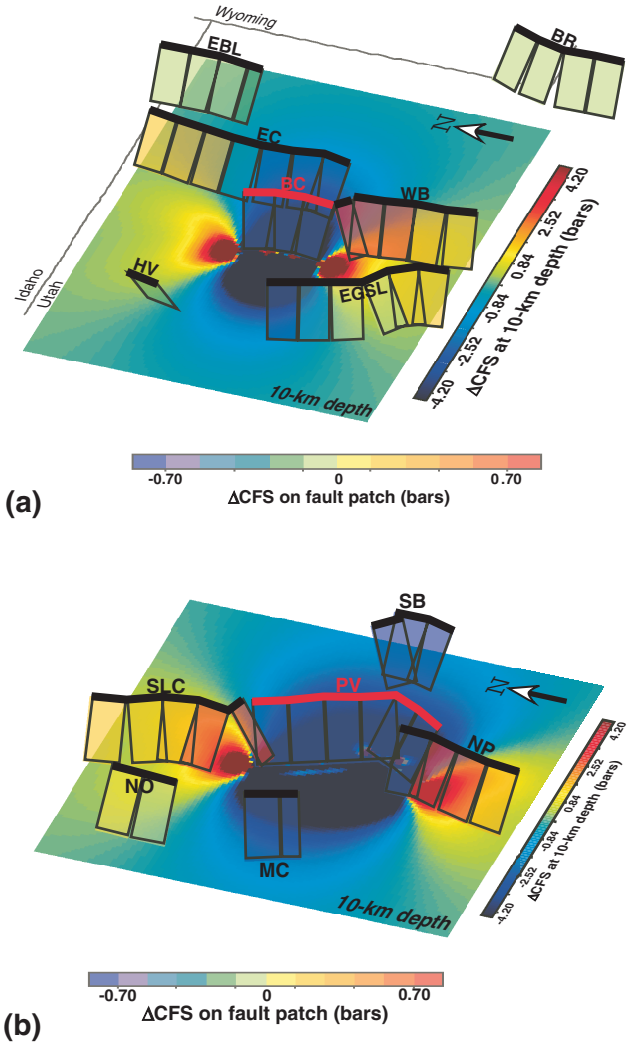

Figure 3. (a) Oblique view showing changes in CFS on adjacent faults and at 10-km depth, induced by scenario earthquakes on: (a) the Brigham City segment (BC; M_s 6.9 or M_w 6.8) and (b) the Provo segment (PV; M_s 7.1 or M_w 7.1). Discretized fault patches are about 10 km long (shown by rectangle). Thick lines show the surface traces of faults, whereas thick, red line represents the ruptured fault.

epicenter alignments, fault geometry, aeromagnetic anomalies, topography, and footwall structure. They concluded that four salients and one gap divide the Holocene-active part of the Wasatch Fault into six segments. We note these defined segments as (from north to south in Fig. 1): Brigham City (BC), Weber (WB), Salt Lake City (SLC), Provo (PV), Nephi (NP), and Levan (LV).

Most of the prominent geometric changes along faults were hypothesized to be segment boundaries, except for a noticeable bend in the PV segment (Fig. 1). Machette *et al.* (1992) pointed out that Holocene faulting continues around the bend, although apparent fault-scarp heights decrease in comparison with the north and the west. The salient between the PV and NP segments, however, is an *en echelon* step,

with no prominent change in fault geometry (Machette *et al.*, 1992; Ostenaa, 1990).

Failure-Stress Modeling

We first examined the ΔCFS induced by a scenario earthquake on the BC segment (Fig. 3a) with a 30-km-long rupture and a displacement of 2 m. This scales to an M_s 6.9 (Mason, 1996) or an M_w 6.8 (Wells and Coppersmith, 1994) normal-faulting earthquake. We chose the BC segment because it has the longest lapse time, ~2,125 years, among the Wasatch Fault segments (McCalpin and Nishenko, 1996), and therefore it is considered to pose the greatest hazard for $M > 7$ earthquakes with up to a 46% chance of occurrence in a 100-year exposure period (McCalpin and Nishenko, 1996)

Figure 3a is an oblique view showing ΔCFS on adjacent fault planes at 10-km depth. It indicates that the WB segment has induced a failure–stress increase of up to 1.2 bars, whereas the East Cache and East Great Salt Lake faults, located east and west of the BC segment, have a stress reduction of up to 5.4 and 0.6 bars, respectively. The pattern of ΔCFS at 10-km depth also shows that the along-strike optimal ruptured planes are loaded by the static stress, while the offstrike (at orthogonal directions) optimal planes are in a stress "shadow."

In addition, ΔCFS was modeled for a scenario earthquake on the longest section of the Wasatch Fault, the PV segment. This event, with a rupture of 60 km long and a displacement of 2 m, corresponds to an M_s 7.1 or M_w 7.1 event (Wells and Coppersmith, 1994; Mason, 1996). Figure 3b shows that the along-strike SLC and NP segments are loaded toward rupture by increased stress up to 1.2 and 4.0 bars, respectively, while the nearby Strawberry and Mercur faults, east and west of the PV segment, are relaxed by 2 bars. The pattern of the regional ΔCFS at 10-km depth also implies that the stress loading would occur around the northern and southern ends of the ruptured segment.

These results suggest that earthquakes on the Wasatch Fault tend to perturb the regional static stress with two plausible consequences: (1) the along-strike (north–south) segments are loaded, reducing their time to the next rupture and (2) segments east and west of the fault are relaxed, increasing their time to the next rupture. These results are compatible with the spatial and temporal distribution of the paleoearthquakes of the Wasatch Front area, of which the Wasatch Fault has experienced a higher rate of earthquakes (17 single-segment events; McCalpin and Nishenko, 1996) than its east–west adjacent faults, which had no more than one event in the past 5.6 kyr (Hecker, 1993; Hylland, 2001). We will later discuss the application of the results of Wasatch Fault stress modeling to earthquake-hazard analyses.

Note that we did not include properties such as the effect of dynamic stress that can be hundreds of times larger than the static stress (e.g., Brune, 1979; Gomberg *et al.*, 1997), fault directivity, and variations in dip on different segments. Knowledge of these factors is largely unknown for the Wasatch Fault and is beyond the scope of this article.

Paleoearthquakes of the Wasatch Fault

Because of the quiescence in historical seismicity clearly associated with the Wasatch Fault (Smith and Arabasz, 1991; Arabasz *et al.*, 1992), geological studies have been an invaluable way to investigate the long-term slip rates of large, scarp-forming paleoearthquakes. These properties, including the space–time distribution, magnitudes, slip rates, recurrence intervals, and probable multisegment ruptures, play important roles in the seismic-hazard assessment.

To examine the spatial and temporal patterns of the paleoearthquakes, we tabulated the age and displacement data from 16 trench sites (Table 1). The six Holocene-active segments of the Wasatch Fault have experienced 17 ruptures in the past 5.6 kyr (lettered in Table 1), according to Jackson (1991) and McCalpin and Nishenko (1996). Note that the surface rupture of event *x* of the WB segment was suggested to die out before reaching the trench site KV-88 (McCalpin *et al.*, 1994). In spite of this exception, all of the other paleoevents were assumed to be characteristic earthquakes, that is, rupture of a single segment.

Moreover, a deep trench excavated in September 1999 across the SLC segment (McCalpin and Nelson, 2001) was important for developing evidence of paleoearthquakes that postdate the abandonment of Lake Bonneville. This mega-trench exposed 26 m of vertical section across a 30-m-wide fault zone containing two subparallel scarps and revealed a 6.0 ± 1.2-kyr period of fault inactivity between ca. 9.0 ka and 15.5 ka ago. This time span is about four to five times longer than the 1.4 ± 0.2 kyr of the average recurrence interval of the SLC segment in the past 5.6 ka (Table 1), which implies that the long-term earthquake occurrence of the Wasatch Fault has been irregular in the past 15 kyr.

The multisegment rupture, on the other hand, is also a plausible working model for the Wasatch Fault, especially when earthquakes on adjacent segments have occurred close in time. For example, in Table 1, the oldest events on the BC (*x*) and WB (*x*) segments could not be distinguished as separate within the error of ages, neither could the oldest events on the SLC (*w*) and PV (*x*) segments. We will next discuss this scenario based on our new analysis of the Wasatch Fault paleoseismic data.

Multisegment Rupturing Model

Although the confinement of fault rupturing has been widely proposed, ruptures that "jump" across boundaries into adjacent segments are common for large earthquakes. The following is an illustration showing how rupture can initiate on a main segment and progress into adjacent segments or rupture from one segment into another:

The Working Group on California Earthquake Probabilities (1995) contended that many past earthquakes on the San Andreas Fault ruptured one or more segments in a single

Table 1
Paleoseismic Data of the Wasatch Fault

Fault Segment	Trench Site*	Age of Trench Event† (cal. yr. B.P.)	NVTD‡ (m)	Age of Single-Segment Event§ (cal. yr. B.P.)
Brigham	BC, T	3,600 ± 500	0.8–~1.35[7]	*z* 2,125 ± 104
City[1,2]		4,700 ± 500	2.5	*y* 3,434 ± 142
	PP	4,600 ± 500	0.7–~1.3	*x* 4,674 ± 108
Weber[1,6]	GC	800–~1,200	1.0	*z* 1,016 ± 62
		1,500–~2,000	1.0	*y* 3,064 ± 114
	EO	800–~1,200	0.9–~2.2	*x* 4,403 ± 122
		2,500–~3,000	2.2–~3.5	
		3,500–~4,000	2.2–~2.5	
	KV-88	600–~800	1.7–~1.9	
		2,800 ± 700	2.3–~3.4	
Salt Lake	SFDC	1,100–~1,500	0.9–~2.7	*z* 1,230 ± 62
City[1,3]		2,100–~2,800	0.5–~3.8	*y* 2,499 ± 138
		3,500–~4,500	0.8	*x* 3,940 ± 216
		4,950–~5,750	1.4–~2.2	*w* 5,381 ± 136
Provo[1,4]	AFC	500 ± 100	2.2–~2.7	*z* 618 ± 30
		2,650 ± 150	2.2–~2.7	*y* 2,842 ± 72
		5,300 (5,289–~5,721)	2.2–~2.7	*x* 5,481 ± 152
	RC	1,005 (950–~1,150)	2.5	
	MN, MS	600 ± 80	1.4–~3.0	
		2,820 (+150/−130)	0.8–~2.8¶	
	WC	1,000 ± 200	0.75–~1.0	
Nephi[1,5]	NC	<1,000–~1,300	2.0–~2.2	*z* 1,148 ± 68
		<4,000 ± 200	2.0–~2.5	*y* 3,864 ± 238
		<5,300 (+600/−700)	2.6	*x* 4,500 ~ 5,000[5]
	RedCyn	1,300 (+200/−300)	1.4 ± 0.3	
		3,000–~3,500	1.5 ± 0.2	
		4,000–~4,500	1.7 ± 0.3	
Levan[1,5]	DC	1,000 ± 100	1.8	*z* 1,000 ± 100[5]
	SP	<1,700 ± 200	2.0	

Cal. yr. B.P., Calendar years before present. Superscripted numerals indicate references.

*Trench or exposure site: BC, Brigham City; T: Provo delta east of Brigham City; PP, Pole Patch; GC, Garner Canyon; EO, East Ogden; KV-88, Kaysville 1998; SFDC, South Fork Dry Creek; AFC, American Fork Canyon; RC, Rock Creek at Provo; MN, Mapleton North; MS, Mapleton South; WC, Water Canyon; NC, North Creek; RedCyn, Red Canyon; DC, Deep Creek; SP, Skinner Peaks.

†Ages of trench events are shown as blank rectangles in Figure 6.

‡NVTD, net vertical tectonic displacement.

§Ages of single-segment events come from McCalpin and Nishenko (1996), except for event *x* of the Nephi segment and event *z* of the Levan segment (Jackson, 1991).

¶Displacement data from the Hobble Creek trench site, about 3 km north of the Mapleton North site.

[1]Machette *et al.* (1992); [2]Personius (1991); [3]Black *et al.* (1995); [4]Lund *et al.* (1991), [5]Jackson (1991); [6]McCalpin *et al.* (1994); [7]personal communication, McCalpin (1997).

event. They defined a "cascade model" for simultaneous ruptures on contiguous segments to calculate the earthquake occurrence rates in the southern California seismic-hazard analysis. Mason (1996) analyzed a worldwide set of historical, normal-slip earthquakes, including the Hebgen Lake and Borah Peak earthquakes specific to the ISB. On the basis of his magnitude scaling of fault length, he suggested that a multisegment model is a better approximation than a single-segment model for estimating the maximum magnitude.

For the extensional Basin–Range province, Wheeler and Krystinik (1992) and Pezzopane and Dawson (1996) proposed that most of the large, historical earthquakes in this regime experienced multisegment surface rupture. Figure 4 shows the along-strike fault displacements and segmentations observed from nine $M \geq 6.5$ Basin–Range earthquakes (Pezzopane and Dawson, 1996), of which eight ruptured more than one segment. These observations suggest that segment boundaries were not barriers for lateral rupture propagation and therefore support the working model of multisegment rupturing for large Wasatch Fault earthquakes.

Figure 5 shows a time–space plot of paleoearthquake data for the Wasatch Fault in which multisegment rupturing is considered. Instead of 17 single-segment events shown in Table 1, there are 11 paleoearthquakes, of which as many as eight dual-segment ruptures are suggested. These multisegment events are easily perceived, based on the range of error in the space–time distribution of trench data shown in Figure 5. We direct readers to a detailed discussion of these scenario events by Chang (1998).

One difficulty, however, with specifying multisegment

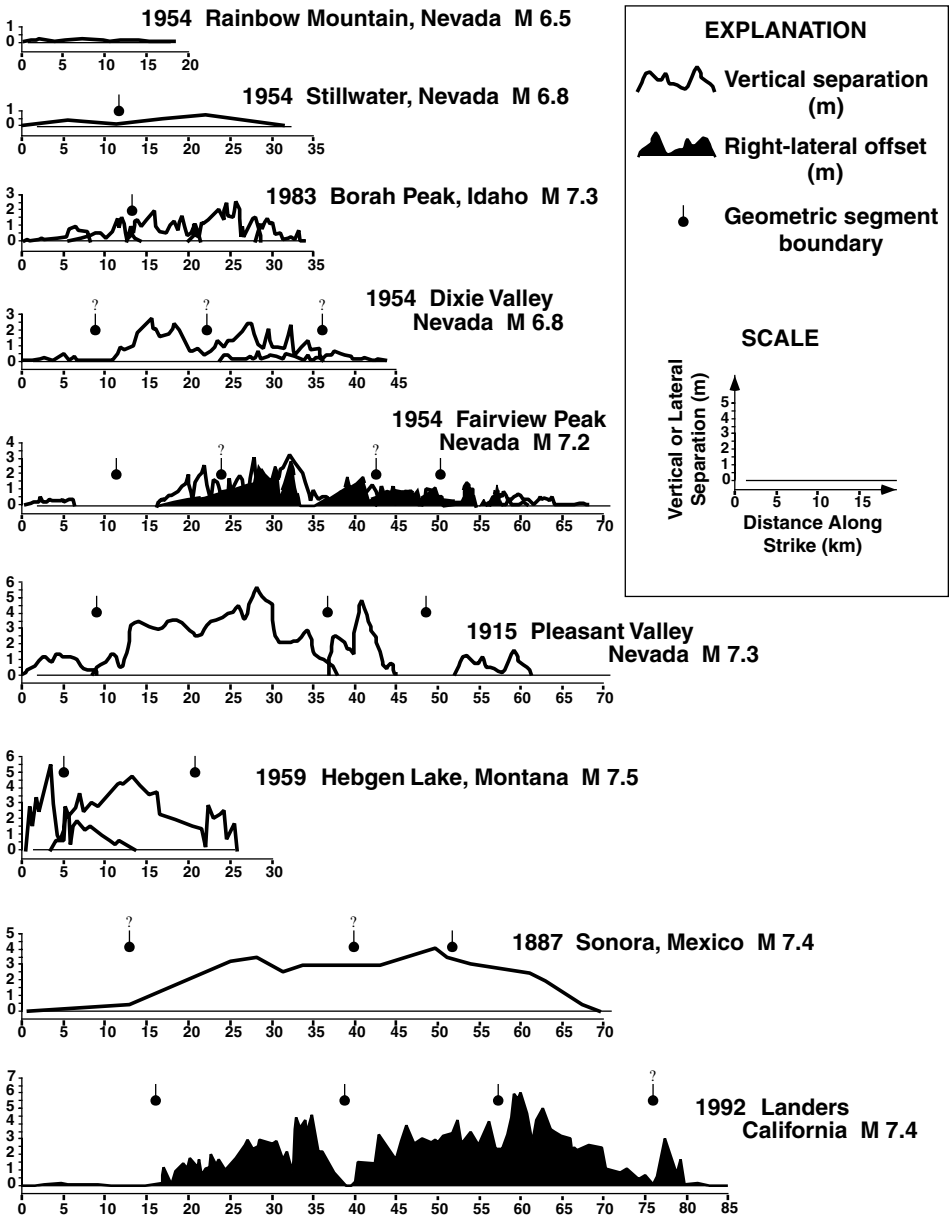

Figure 4. Along-strike fault displacements and segments of scarp-forming Basin–Range earthquakes (taken from Pezzopane and Dawson, 1996). Note that essentially all of these earthquakes experienced multisegment ruptures (except for the 1954 Rainbow Mountain, Nevada, earthquake). The observations corroborate the use of an elliptical distribution as a first-order approximation for the along-strike fault displacement.

ruptures on the central Wasatch Fault was the lack of uniform paleoseismic information, especially the ~60-km gap of trenching information between the southern SLC and WB segments (Fig. 5). This questions the assumption of continuous faulting of paleoearthquakes on the SLC segment. Because of this uncertainty, events A, D, G, and I in Figure 5 were taken as the upper-end members of the range in size.

In summary, we suggest that multisegment rupturing is a good working model for large Wasatch Fault earthquakes, based on our analysis of the paleoearthquake trenching data. Compared with single-segment ruptures, the multisegment scenario contains fewer but larger-magnitude events. In the following section, we will estimate the total seismic moment and the frequency of occurrence of both scenarios, and then address their implications to seismic-hazard analyses.

Wasatch Front Integrated Seismic-Hazard Estimations

Traditionally, probabilistic seismic-hazard estimation for the Wasatch Front area has employed geological fault-slip rate and historical seismicity data. Slip rates were esti-

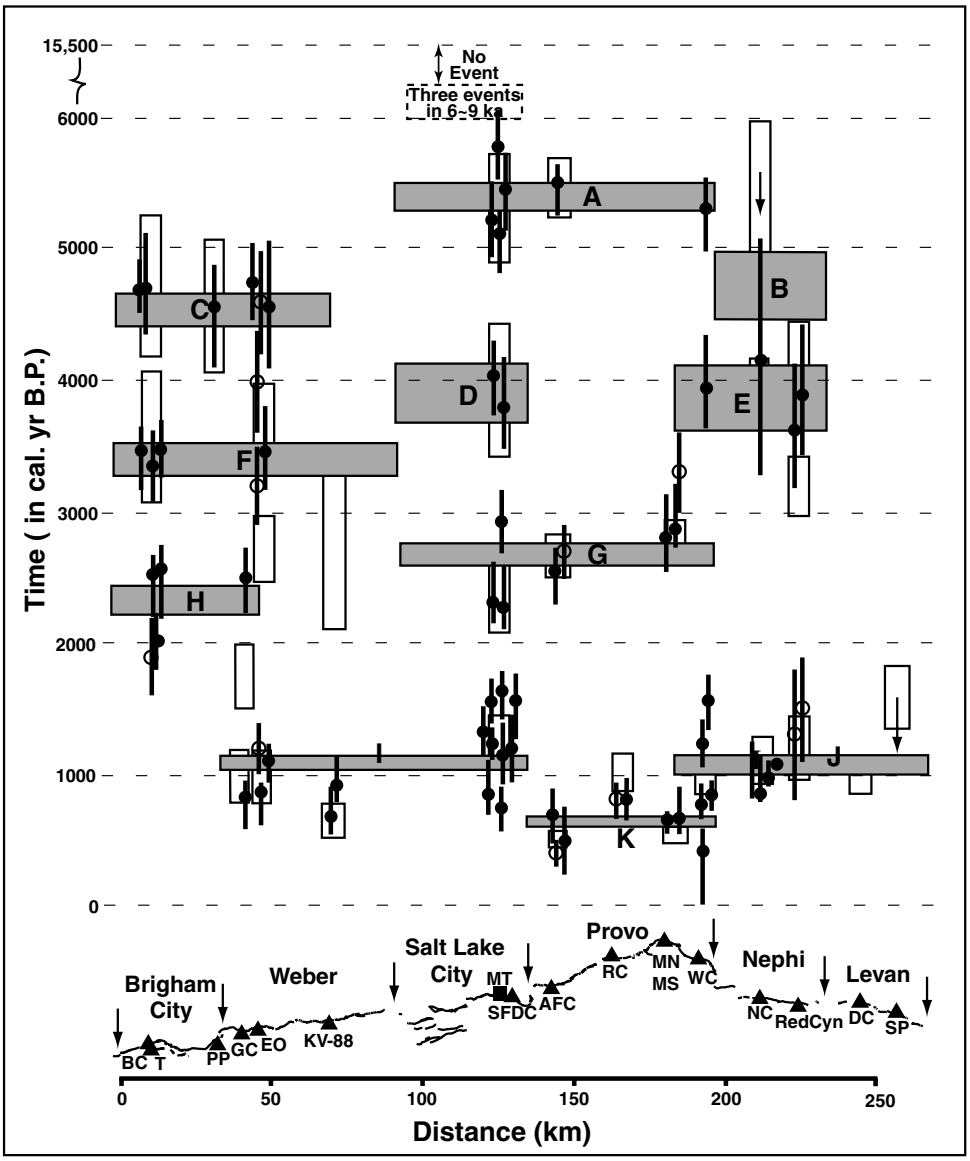

Figure 5. Space–time distribution of multisegment paleoearthquakes on the Wasatch Fault assumed by this study. There are as many as eight dual-segment ruptures (events A, C, E, F, G, H, I, J). Trench sites listed in Table 1 are shown by triangles. Black bars represent numerical ages from McCalpin and Nishenko (1996), with averages shown by dots (C^{14} dating) and circles (thermoluminescence dating). Hollow boxes represent paleoearthquakes determined from trenching (see Table 1). Each lettered gray box indicates a multisegment rupture. Notice that a newly excavated megatrench (MT, shown by a square; McCalpin and Nelson, 2001) on the Salt Lake City segment revealed a 6–7-ka period of tectonic quiescence between 9 and 15.5 ka ago (dashed box).

mated from the ages and displacements of scarp-formed, single-segment paleoearthquakes. For example, the U.S. National Seismic Hazard Maps (Frankel *et al.*, 1996) applied these data compiled up to the mid 1990s. Wong *et al.* (1995) evaluated the hazard of a mine-tailings pond in the Salt Lake Valley by using a compilation of similar data. The most recent work by Wong *et al.* (2001) developed microzonaton maps that depict ground shaking generated by a scenario M_w 7.0 earthquake on the SLC segment of the Wasatch Fault.

In this study, we introduced additional factors, namely, multisegment rupturing, fault-stress contagion, and contemporary crustal deformation, as an example of a more complete estimate of earthquake hazard on the Wasatch Front, Utah. We first applied an elliptical fault-displacement distribution to model the maximum displacement and magnitude of each single-segment and multisegment paleoearthquake. Different occurrence rates of large earthquakes (M >6.6) on the Wasatch Fault were estimated based on the

sizes of paleoearthquakes, the fault-slip rates, and the GPS-implied horizontal extensional rates. We then plotted earthquake peak ground acceleration (PGA) hazard curves for a test site near Salt Lake City by using the aforementioned occurrence rates and including the effect of fault–stress interaction.

Paleoearthquake Parameterization

For an ideal fault in a homogeneous medium, fault displacement varies from a maximum at the center of the fault surface to zero at the tip. Although most detailed slip models are very heterogeneous, empirical observations (Fig. 4) suggest the use of an analytic half-ellipse as a first-order approximation for the along-strike fault displacement of Basin–Range normal-faulting earthquakes (Olig, 1994; Pezzopane and Dawson, 1996). We thus employed an elliptical slip distribution for Wasatch Fault paleoearthquakes.

Figure 6a and 6b shows the interpreted single-segment and multisegment paleoearthquakes, respectively, of the Wasatch Fault, along with their ages, locations, and displacements that are fitted analytically by half-elliptical envelopes with their semimajor axes as fault lengths and the semiminor axes as fault displacements. By using the total rupture length, maximum displacement (scaled by the maximum height of each ellipse), and magnitude of each event, the total seismic moment is 4.2×10^{20} N-m for 17 single-segment ruptures (Fig. 6a) and 4.7×10^{20} N-m for 11 multisegment ruptures (Fig. 6b). The average magnitude of single-segment earthquakes, on the other hand, is about 0.1 less than that of the multisegment events. These close values imply that both scenarios preserve moment from the point of view of paleoseismic moment budget.

Wasatch Fault Slip Rates

Fault-slip rate is perhaps the most important factor in earthquake-hazard assessment because it is an estimate of how fast seismic energy is accumulated. For two consecutive paleoearthquakes, we defined the interevent slip rate as the maximum fault displacement divided by the time between two earthquakes and will use this definition throughout. Because of the relatively small number of paleoearthquakes on the Wasatch Fault, we added an additional estimate of slip rate by considering an end-member occurrence, using the time since the last event to the present. For this estimate, we assumed a scenario earthquake with a 2-m displacement, corresponding to an M_w 7.1 event (Wells and Coppersmith, 1994), could occur any time in the future, with the present being the youngest.

The interevent and end-member slip rates corresponding to the single-segment and multisegment scenarios, together

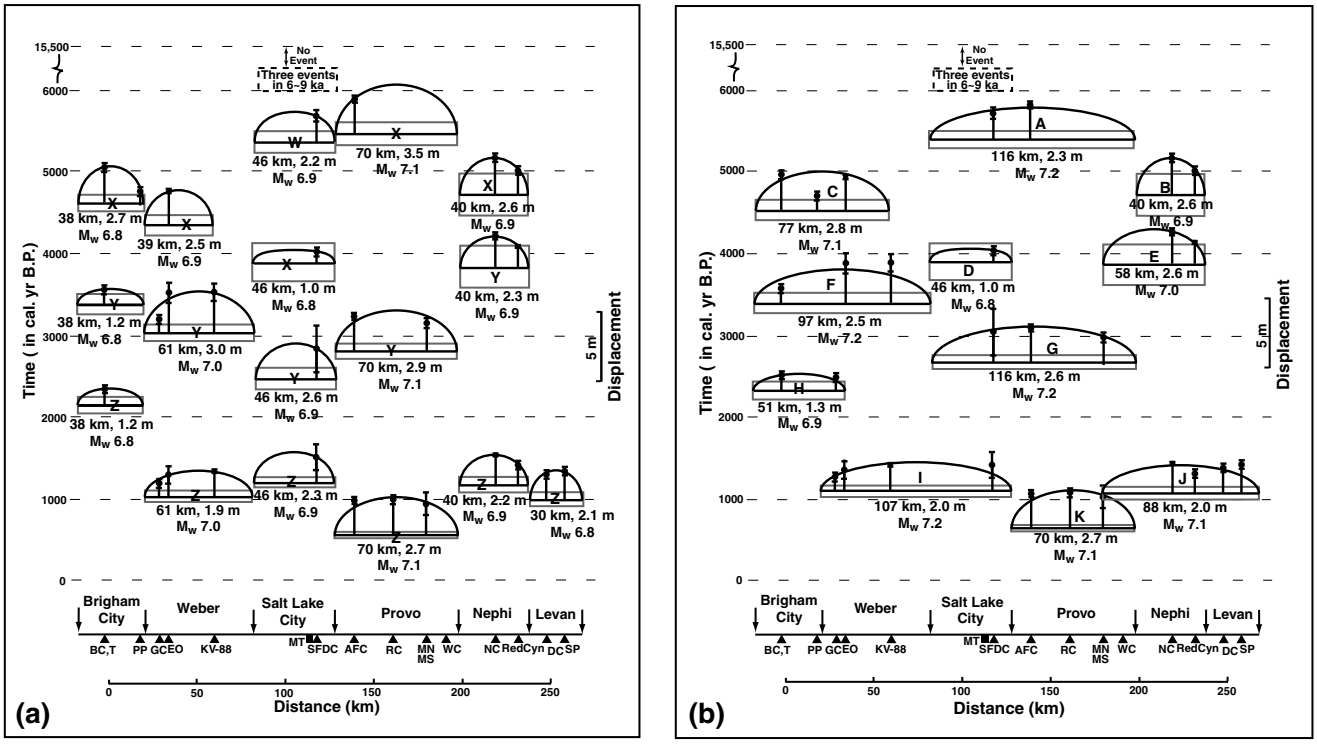

Figure 6. Modeled distributions of fault slip based on (a) single-segment and (b) multisegment paleoearthquakes of the Wasatch Fault. Vertical black lines show averages (dots) and errors (between tics) of fault-slip data measured from trenches (see Table 1). For each event, fault displacements are fitted by a semi-elliptical envelope (see text for discussions). The rupture length, maximum displacement, and moment magnitude, shown for each event, are scaled from Wells and Coppersmith (1994) and Mason (1996).

with their averages and standard deviations, are shown in Table 2 for different segments of the Wasatch Fault. The average slip rate ranges from 1.0 to 1.9 mm/yr for our preferred multisegment rupturing model and 0.9 to 1.8 mm/yr for the single-segment model. Note that the 6–7-ka period of fault inactivity exposed by the megatrench (McCalpin and Nelson, 2001) implies a low slip rate, ~0.3 mm/yr, with constant loading assumed, on the SLC segment between ~15.5 ka ago and the first Holocene faulting event (~9.0 ka ago). These variations suggest that slip rates along the fault are temporally and spatially irregular, that is, with rates on the order of the errors.

Stress Contagion

Modeling the change of the failure stress can also be used to infer the earthquake probability based on a prediction of expected stress loading on faults. In the first example of this method, Cornell *et al.* (1993) related the induced failure stress to the temporal change of the next event by using elastic dislocation analyses. They also derived analytical expressions for future probabilistic earthquake risk, conditional on the elapsed times and the number of events of relevant fault segments. In addition, Stein *et al.* (1997) applied the Coulomb failure condition to earthquake probability estimations on the North Anatolian Fault, Turkey. On the basis of the aftershock data of the 1995 M_w 6.9 Kobe, Japan, earthquake, Toda *et al.* (1998) also investigated the transient effects of stress changes that are incorporated by the rate-and-state constitutive relation (Dieterich, 1994; Dieterich and Kilgore, 1996). They concluded that these transient effects amplify the permanent (or time-independent Coulomb) stress changes during the aftershock period and thus alter the probability of subsequent events over a distance of several fault lengths and a period of several times the aftershock duration.

As a first-order estimation to the Wasatch Fault, we employed the methodology developed by Cornell *et al.* (1993) that takes into account the change in rupture probability caused by the time-independent Coulomb stress change. Figure 7 shows an example for the SLC segment that currently has an elapse time (time to the last rupture) of 1,230 years (status I). If the adjacent WB and PV segments rupture now, the SLC segment would be loaded by an induced stress ΔCFS, and the time to its next failure will be advanced by Δt (status II, Fig. 7). Thus, the probability of SLC rupture in the next 50 years will be increased, from 2.1% to 4.8%, 3.2% to 3.6%, and 2.6% to 3.7%, respectively, based on the time-dependent lognormal ($\sigma_D = 0.21$ and $\sigma_D = 0.5$) and Weibull recurrence models (Fig. 7). The stress contagion, however, will not affect the rupture probability if a time-independent Poisson-recurrence model is applied.

Temporal changes of earthquake hazard that are caused by time-dependent stress evolutions on faults need to be evaluated quantitatively by time-dependent methods, such as viscoelastic modeling (a topic that we are working on for another study). Viscoelastic modeling that includes the ef-

Table 2
Slip Rates of the Wasatch Fault

Fault Segment	Segment Scenario	Interevent Slip Rate (mm/yr) IV*	III*	II*	I*	EMSR*	Average Slip Rate (±1 σ)
Brigham City	Single			1.0	0.9	0.9	0.9 ± 0.04 (0.9 ± 0.03)†
	Multiple			1.9	1.2	0.9	1.5 ± 0.5 (1.3 ± 0.5)
Weber	Single			2.2	0.9	2.0	1.6 ± 0.9 (1.7 ± 0.7)
	Multiple			1.9	0.9	2.0	1.4 ± 0.7 (1.6 ± 0.6)
Salt Lake City	Single	0.6	0.7	1.8	1.8	1.6	1.2 ± 0.7 (1.3 ± 0.6)
	Multiple	0.6	0.7	2.0	1.6	1.6	1.2 ± 0.7 (1.3 ± 0.6)
Provo	Single			1.1	1.2	3.2	1.2 ± 0.1 (1.8 ± 1.2)
	Multiple			0.9	1.2	3.2	1.0 ± 0.2 (1.8 ± 1.3)
Nephi	Single			2.6	0.8	1.7	1.7 ± 1.3 (1.7 ± 0.9)
	Multiple			2.9	0.9	1.7	1.9 ± 1.4 (1.8 ± 1.0)

*I, II, and III represent the first (latest), second, and third interevent slip rate, respectively. IV is the rate based on the megatrench event of the Salt Lake City segment. EMSR, the end-member slip rate, is defined as 2m/(age of the most recent event of each segment).

†Average slip rates in parenthesis are calculated with EMSR included.

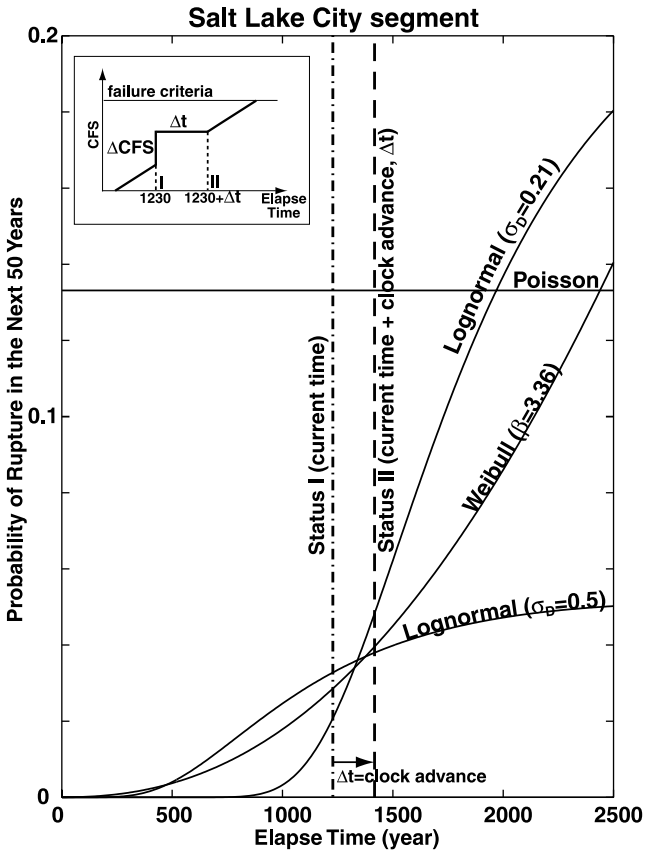

Figure 7. Effect of stress contagion on the probability of rupture of the Salt Lake City segment, Wasatch Fault, with an elapsed time of 1,230 years. Dot–dashed and dashed lines represent the current status (status I) and the status after clock advance due to the stress increase caused by ruptures on the adjacent segments (status II), respectively. Different models of recurrence interval are shown. Insert diagram shows how induced stress (ΔCFS) can disturb stress accumulation on fault (thick, solid line) and in turn advance the time (Δt) to the next rupture.

fect of long-term stress relaxation on the upper mantle could better explain time delays between mainshock and subsequent events, as well as irregular recurrence intervals (e.g., Pollitz and Sacks, 1997). We are currently evaluating time-dependent models, but they are beyond the scope of this article.

Earthquake Recurrence from Seismic, Geologic, and Geodetic Observations

Among different recurrence models that were proposed by McCalpin and Nishenko (1996) for the Wasatch Fault paleoearthquakes, the stationary Poisson model may not be suitable for earthquake recurrence. The lognormal and Weibull renewal models both imply a time-dependent failure rate; however, we favor the lognormal distribution because it was found to provide a better fit to the earthquake-recurrence intervals for events from a number of plate boundaries (Nishenko and Buland, 1987). McCalpin and Nishenko (1996) used 0.21 and 0.50 for the intrinsic variability (σ_D, the ratio of the standard deviation to the mean), in which a lower value implies a more-regular recurrence behavior of the fault. Figure 7 shows that the rupture probability increases by about a factor of 2.3 and 1.1 for σ_D 0.21 and 0.50, respectively, with the stress-contagion effect taken into account.

The relation between the number and magnitude of earthquakes can be generally described by two commonly used models: the characteristic and truncated-exponential. The characteristic model implies that a fault tends to repeat similar sizes of large earthquakes whose recurrence intervals are described by probability distribution functions (e.g., Schwartz and Coppersmith, 1984; Youngs and Coppersmith, 1985; Wesnousky, 1994). The truncated-exponential model, on the other hand, suggests a modified Gutenberg–Richter relation, in which no event will occur above an upper-magnitude bound (Cornell and Van Marke, 1969).

Figure 8 outlines the Holocene-active faults of the Wasatch study area. Following the definitions by the Working Group on California Earthquake Probabilities (1995), we categorized these faults into two types: type A faults, whose paleoseismic data suffice to estimate conditional probabilities, and type B faults, which have insufficient data for conditional probability analysis, so that their frequencies of occurrence are obtained from slip rates and the maximum magnitudes. In the Wasatch study area, we chose five type A and 10 type B faults or fault segments (Fig. 8) that could cause significant earthquake ground shaking in the Salt Lake City urban area.

Figure 8 also shows the historical seismicity of the Wasatch study area that was classified as a type C source. These earthquakes were assumed to be randomly distributed in space and follow the truncated-exponential recurrence model (Appendix). The polygon in Figure 8 marks the Wasatch Fault area, where earthquakes in this region are likely related to the Wasatch Fault. Note that we excluded the 1975 Pocatello Valley, Idaho, earthquake ($M_L = 6.0$) and its aftershocks, which were not considered to be associated with the Wasatch Fault (Chen, 1988; Doser, 1989).

Two independent methods of earthquake declustering, the empirical time and space windows (Youngs *et al.*, 1987) and the ZMAP algorithm (Wiemer, 1996), consistently identified 43 independent mainshocks ($2.0 \leq M_w \leq 4.0$) with a b-value of 0.76 ± 0.07 (from ZMAP) in the Wasatch Fault area. This value is comparable to 0.72 ± 0.06 proposed by Pechmann and Arabasz (1995) employing the maximum-likelihood method for the Wasatch study area, with 61 independent events in the range $3.0 \leq M_L \leq 6.67$ ($2.1 \leq M_w \leq 5.8$). Figure 9 shows that the truncated-exponential curve of the Wasatch Fault ($a = -0.15$, $b = 0.76$) is close to that of the Wasatch study region ($a = -0.26$, $b = 0.72$).

Because moderate to large earthquakes ($M_w > 6.6$) have not occurred on the Wasatch Fault in historical time, the frequency of occurrence of these large events was estimated

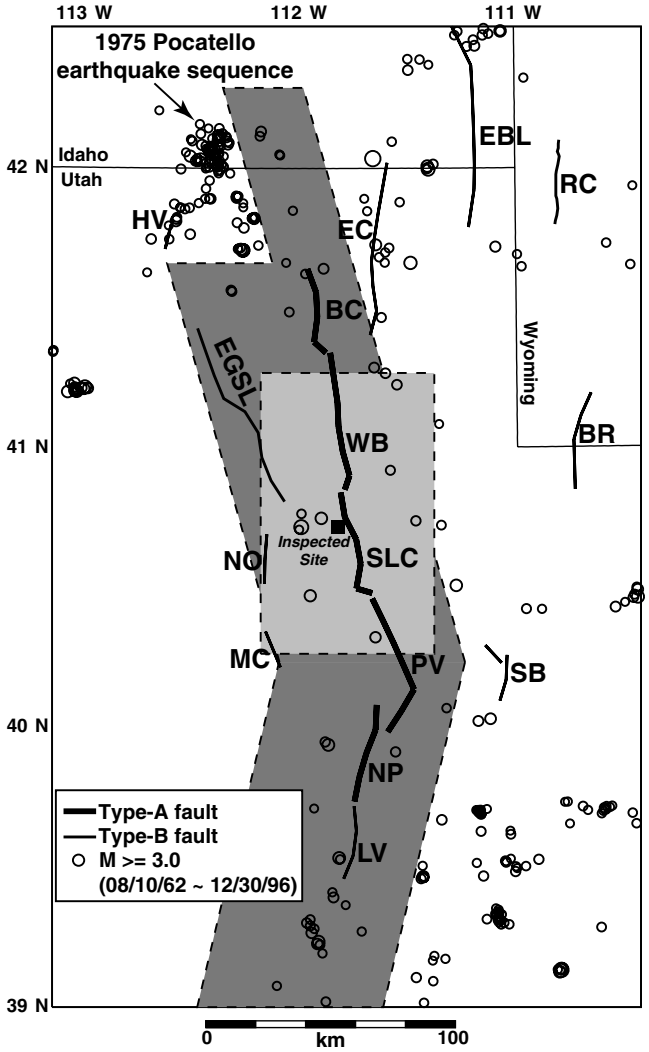

Figure 8. Map showing the locations of earthquakes, with dependent events removed by declustering with magnitude larger than 3.0 (circles) from 10/08/62 to 30/12/96 of the Wasatch Front study area (see text for details of declustering). Earthquakes located within the dark-gray polygon are likely related to the Wasatch Fault. Light-gray rectangle shows the area of 1992–1995 Wasatch Front geodetic surveys. Thick and thin lines represent type A and type B faults, respectively. The small, black square shows the inspected site for the earthquake ground-shaking hazard estimation.

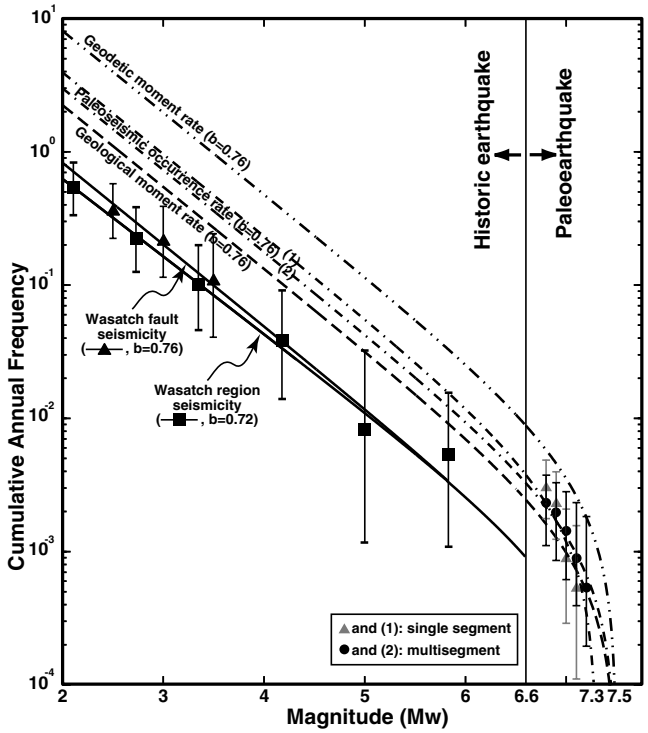

Figure 9. Earthquake recurrence models for the Wasatch Fault. Paleoearthquake information, based on single (dot–dashed line 1) and multiple (dot–dashed line 2) segment scenarios, were used for estimating the recurrence of large events. Note that the minimum threshold for scarp-forming earthquakes in this area is about $M_w > 6.6$. The truncated exponential curves, on the other hand, were fitted to data for (1) the historical seismicity (1962–1996, solid lines), (2) geological moment from fault-slip rates (dashed line, $b = 0.76$), and (3) geodetic moment from the Wasatch Front geodetic observations (dot–dashed line, $b = 0.76$). For the historical seismicity, the b-values of 0.76 and 0.72 were derived from the earthquake catalogs of the Wasatch Fault (the polygon in Fig. 8) and the Wasatch Front regions (Pechmann and Arabasz, 1995), respectively.

based on the paleoseismic record. Figure 9 shows two truncated-exponential recurrence curves ($b = 0.76$) that fit the cumulative annual rates of 17 single-segment (dash–dot line 1, $m_u = 7.3$) and 11 multisegment (dash–dot line 2, $m_u = 7.5$) ruptures. With the same b-value of 0.76 that was derived from the historical seismicity of the Wasatch Fault area (Fig. 9), the a-values implied from the paleoearthquake data ($M_w > 6.8$) are about a factor of 3 higher than that implied from the historical seismic record ($2.0 \le M_w \le 4.0$).

Geological moment, which is obtained from fault-slip rate and can be transformed to the number of earthquake for a given magnitude interval (Appendix), can also be used to estimate earthquake recurrence. On the basis of the multisegment slip rates listed in Table 2, we summed the moment rate of each segment of the Wasatch Fault, distributed the total moment to earthquakes with M_w between 6.6 and 7.5, and then derived a recurrence curve based on the truncated-exponential model (dashed line in Fig. 9). Results show that the annual frequencies of $M_w > 6.6$ events derived by the fault-slip rates are consistent with those implied by the rates of paleoearthquakes (dash–dot lines 1 and 2 in Fig. 9), which are about three times higher than those obtained from the historical seismicity. We will next address some possibilities regarding the discrepancy between the paleo and historical statistics for the Wasatch Fault.

First, the rates of large ($M_w > 6.6$) earthquakes may be

overestimated, because we maximized the magnitudes of Wasatch paleoearthquakes. That is, by breaking one single-segment or multisegment rupture inferred from two or three coeval displacements in trenches into two or three smaller earthquakes in a triggered sequence, would it be possible to fit the paleoearthquake rates to the recurrence curves implied by the historical seismicity?

To address this question, we extrapolated the recurrence curves of historical seismicity shown in Figure 9 (solid lines) to $M_w = 6.6$, the commonly used minimum-threshold magnitude of surface-ruptured earthquakes in the Basin–Range province (Arabasz *et al.*, 1992; dePolo, 1994). The cumulative annual frequency for this magnitude level is about 10^{-3} and corresponds to six events in a period of 6 kyr. This scenario is unlikely, however, because the total of six events is not sufficient to fit the time–space distribution of paleoearthquake data of the Wasatch Fault (Figs. 5 and 6).

Second, the discrepancy could be attributed to the incompleteness of the earthquake catalog, for example, the lack of mid-size earthquakes ($4.0 \leq M_w \leq 6.6$) on faults that have long recurrence cycles but have not been sampled sufficiently in time for best estimates of a full cycle. Alternatively, the Wasatch Fault may have experienced a temporal cluster of rupturing in the past 5.6 kyr (McCalpin and Nishenko, 1996), which caused a higher rate of large earthquakes contrasted with the low historical seismicity.

The last, and also our best, explanation for the rate discrepancy is based on the "characteristic earthquake distribution" (e.g., Wesnousky *et al.*, 1983; Schwartz and Coppersmith, 1984; Wesnousky, 1994) wherein it can be argued that the time between maximum-size earthquakes along faults or fault segments has generally low-level background seismicity, except for the occurrence of foreshocks and aftershocks. Schwartz and Coppersmith (1984) concluded that, for the Wasatch Fault, "linear extrapolation of the recurrence relationship from the lower magnitudes tends to underestimate the frequency of occurrence of the large, characteristic events" (see Fig. 15 of Schwartz and Coppersmith, 1984). If earthquakes on the Wasatch Fault indeed follow the characteristic-earthquake model instead of the Gutenberg–Richter relation, then the discrepancy between the rates of historical seismicity and paleoearthquakes (Fig. 9) could be due to the mechanical behavior of the fault.

We also examined the implication of the contemporary deformation rate determined by GPS measurements on the Wasatch Front (Martinez *et al.*, 1998; Chang *et al.*, 2000). Geodetic moment rate, which indicates how fast energy is being accumulated in a given crustal volume, can be calculated from strain rate if the strain is assumed to be elastic within the seismogenic upper crust (Kostrov, 1974; Ward, 1998).

For the Wasatch Front, a campaign-style GPS survey area is 55 km wide and 100 km long, including the SLC segment and a part of the WB and PV segments (Fig. 8). Data from four GPS surveys (1992–1995) and other geodetic measurements (1962–1991) revealed a strain rate of 49 ± 23 nstrain/yr, which corresponds to a horizontal extension rate of 2.7 ± 1.3 mm/yr (Martinez *et al.*, 1998). This result was corroborated by the 1996–1999 continuous GPS observations on the Wasatch Front (Chang *et al.*, 2000).

If we assume an end-member scenario in which the Wasatch geodetic moment is totally loading the Wasatch Fault, then the annual rate of $M_w \geq 6.6$ earthquakes on the fault would be about four times higher than that derived by the geological moment and paleoseismic occurrence (dash–dash–dot line in Fig. 9). On the basis of the cumulative moment of historical seismicity on the northern Wasatch Front, however, Eddington *et al.* (1987) proposed a strain rate of 0.0041 μstrain/yr that corresponds to a horizontal deformation rate of 0.13 mm/yr and is about 10 times lower than the geodetic strain rate (Martinez *et al.*, 1998). This inconsistency implies that the accumulated strain energy due to contemporary crustal deformation may not have been entirely released by earthquakes. Other aseismic mechanisms, such as fault creep within the ductile part of the crust (Lavier *et al.*, 2000), may be responsible for dissipating part of the strain energy.

Integrated Ground-Shaking Seismic-Hazard Assessment

We have discussed here an example of an integrated, probabilistic seismic-hazard analysis that combines seismic, geologic, and geodetic data of the Wasatch Front area. We calculated hazard values for a single point in the center of the Salt Lake Valley that is a good approximation for hazard within the populated cities on the alluvium-filled valley of the Wasatch Front to demonstrate our ideas. The calculation was made for a location at the intersection of Interstate highways I-15 and I-80 (longitude 111.9° W, latitude 40.7° N; Fig. 8) and is classified as a soil site.

We used only the seismic-attenuation equation SEA99 (Spudich *et al.*, 1997; Spudich *et al.*, 1999) for the Wasatch Front hazard analysis, although we recognize that other attenuation relationships, such as those of Abrahamson and Silva (1997) and Campbell (1997), can also be applied to normal-faulting earthquakes. The new relationship of Spudich *et al.* (1999) was developed for extensional-strain regimes of normal- to oblique-faulting earthquakes. It implies a 10%–20% reduction in peak ground accelerations compared with standard relationships for strike-slip and thrust-event regimes.

For the recurrence of type A sources, lognormal (renewal) distribution functions were used on each fault segment for fitting the interevent times of single-segment earthquakes (McCalpin and Nishenko, 1996). We also included the stress-contagion effect in the estimation of ground-shaking hazard. To avoid overestimating the magnitude of multisegment earthquakes, we allowed only 15 km of rupture into adjacent segments. For example, we quantified the stress contagion of the SLC segment by estimating the conditional probabilities of simultaneous ruptures on SLC and

15 km of WB; SLC and 15 km of PV; and SLC and 15 km of WB and PV.

Figure 10 shows the ground-shaking hazard curves, or the annual frequency of PGA (horizontal) exceedance, corresponding to different types of source (Fig. 8 and Appendix). The SLC segment is expected to contribute the highest seismic hazard to the inspected site owing to its proximity to Salt Lake City. For example, because SLC has an elapsed time of 1,230 years since the last large event and is close to its average repeat time (~1,400 years for a segment-specific model), the lognormal model will present a higher probability of PGA exceedance than the stationary Poisson model does. Smaller σ_D (0.21), which implies more periodic earthquake occurrence, will give a higher PGA compared with $\sigma_D = 0.5$ because the elapsed time of SLC is close to its average repeat time. Among these models, we favor the lognormal with $\sigma_D = 0.5$ because the overall interevent times of Wasatch paleoearthquakes do not seem regular (the coefficient of variance is 0.66 from McCalpin and Nishenko, 1996).

Including the geodetic moment introduces a higher rate on regional, random earthquakes (type C sources) and therefore notably increases the probability of exceedance of small PGA. In Figure 10, for example, the annual probability of PGA $\geq 0.3g$ is increased by about a factor of 2 if the geodetic moment is taken into account (solid line with circles). We caution the reader, however, that the earthquake rate can be proportionally lower if some of the seismic-energy accumulation implied by the GPS measurements has been dissipated by aseismic creep, or if the postseismic deformation due to viscoelastic relaxation is taken into account. Therefore, we considered the geodetic-moment rate to be an upper-bound estimate to the background seismicity rate.

Moreover, including the stress-contagion effect will increase the probability of exceedance of large PGA, for example, about a factor of 2 for PGA $\geq 0.5g$ in Figure 10. Note that compared with the single-segment model, stress contagion introduces larger earthquakes, of which the probability of occurrence (or occurrence rates) should be lower in order to balance the long-term moment of the earthquake catalog. Therefore, we applied the single-segment recurrence model to stress contagion only for an upper-bound estimate to the seismic hazard. Figure 10 shows that with stress contagion, increasing the mean recurrence interval of SLC from 1,767 years (thick dashed curve), derived from the single-segment rupturing scenario (McCalpin and Nishenko, 1996) to 2,100 years (thin dashed curve) would decrease the probability of PGA $\geq 0.5g$ by about a factor of 1.3.

Overall, various earthquake sources contribute differently to the ground-shaking probability estimation. As an example, we estimated the annual frequency of exceedance of $0.25g$, the commonly acknowledged lower threshold of PGA in causing damage on normal structures, from the hazard curves shown in Figure 10. Compared with the historical seismicity curve that is considered as the lower bound (thick solid curve), including the paleoearthquakes, geodetic strain rate, and upper-bound stress contagion would increase the annual frequency of PGA $\geq 0.25g$ by a factor of 1.4, 4.0, and 5.4, respectively.

Conclusions

This is the first study using elastic-stress modeling to evaluate the effect of stress interaction on large, normal-faulting earthquakes in the ISB, including the two largest,

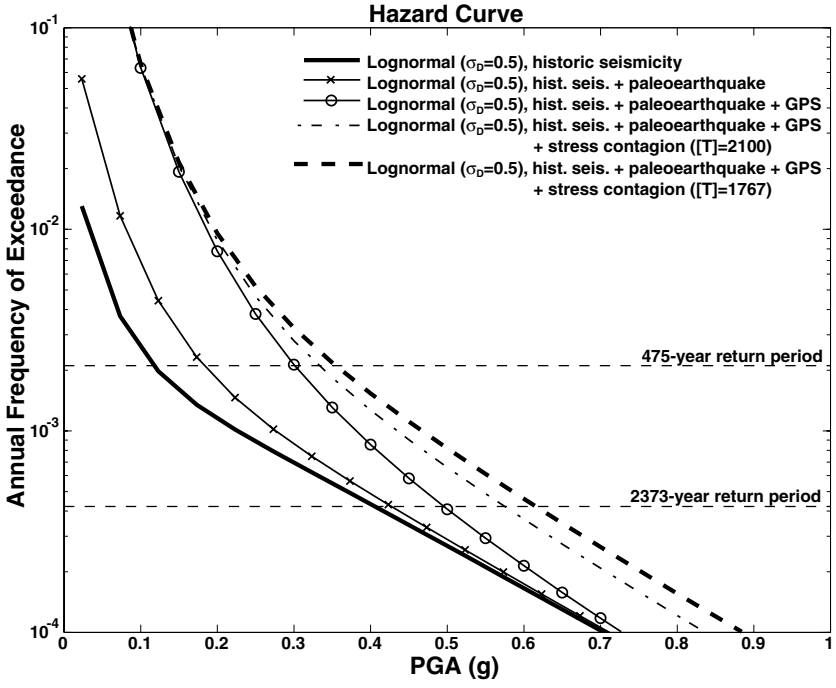

Figure 10. Example of the integrated seismic hazard for a soil site near Salt Lake City, Utah (111.9°W, 40.7°N; Fig. 8) showing the annual frequency of peak ground acceleration (PGA) exceedance. The fault-specific lognormal distribution ($\sigma_D = 0.5$) was used for the recurrence of the Wasatch Fault, with the stress-contagion effect included, assuming 15-km induced ruptures on adjacent segments. For random earthquakes, we assumed truncated exponential models ($b = 0.76$) based on historical seismicity, geological moment rate, and geodetic moment rate. Also, we employed the PGA attenuation for extensional regimes of Spudich *et al.* (1999). Note that two mean recurrence intervals ([T]) were tested for including the stress contagion (see text for explanations).

historical events and the paleoearthquakes of the Wasatch Fault. Results of modeling the 1959 Hebgen Lake (M_s 7.5) and the 1983 Borah Peak (M_s 7.3) earthquakes showed a positive correlation between areas of increased failure stress and areas of extended aftershocks. The Hebgen Lake earthquake likely triggered not only large ($M > 5.5$) aftershocks several years later but also numerous earthquakes adjacent to the Yellowstone caldera. The prominent increase of background seismicity north of the Lost River Fault after the 1983 Borah Peak earthquake was also explained by increased stress.

These examples suggest that the failure–stress methodology explains aftershock sequences of large events in extensional stress regimes. The method was then applied to the historically seismically quiescent Wasatch Fault to assess the effect of stress change on the space–time patterns of paleoearthquakes. Results showed that the along-strike (north–south) segments are loaded, while side (east–west) segments at 90° to the rupture can be relaxed by induced failure stress. The multisegment rupture model for the Wasatch Fault suggests 11 paleoearthquakes in the past 5.6 kyr, of which as many as eight events ruptured across identified segment boundaries.

We then examined the frequency of earthquake occurrence on the Wasatch Fault by using a truncated Gutenberg–Richter relation. The cumulative frequency of $M_w > 6.6$ earthquakes estimated by late-Holocene paleoearthquakes is about a factor of 3 higher than that obtained by historical seismicity. This difference suggests that (1) large, scarp-forming earthquakes in the past 5.6 ka on the Wasatch Fault may be temporally clustered; (2) the historical record is too short to provide an accurate estimate of a complete seismic cycle; or (3) earthquakes on the Wasatch Fault follow the characteristic-earthquake model. The higher geodetic-moment rate, contrasting with the low, historical seismic-moment rate of the Wasatch Front, suggests that aseismic moment due to fault creep or other aseismic mechanism may be significant, or it may indicate an irregularly high interseismic stress loading.

The Wasatch Front seismic, geologic, and geodetic data were then included in an integrated probabilistic earthquake-hazard calculation for a specific location in the Salt Lake Valley to demonstrate the usefulness of employing all available data for a more complete estimate for the entire region. Compared with the historical seismicity hazard curve that is considered to be the lower bound, including the paleoearthquakes, geodetic strain rate, and upper-bound stress contagion would increase the annual frequency of PGA $\geq 0.25g$ by a factor of 1.4, 4.0, and 5.4, respectively.

We note that the stress modeling used in this study has assumed elastic, or time-independent, stress change. For long time periods such as the hundreds to thousands of years that would be necessary to evaluate an entire earthquake cycle in low stress-loading regimes like the Basin–Range Province, it is more appropriate to contain time-dependent effects, such as long-term viscoelastic loading and relaxation of the Earth's lithosphere, and is the subject of future research.

Acknowledgments

We thank Bob Simpson for assisting us on the use of his boundary-element code and discussing the results with us. Jim McCalpin provided data insights, discussions, and preprints of his work on prehistoric earthquake behavior of the Wasatch Fault. Chuck Meertens offered his knowledge on the crustal deformation of the Wasatch Front area. Discussions and data from Gary Christenson, David Schwartz, and Michael Machette benefited this paper. The research was funded by the University of Utah Mineral Leasing Funds and the U. S. Geological Survey (USGS), Department of the Interior, under NEHRP (National Earthquake Hazards Reduction Program) award No. 1434-HQ-96-GR-02746. The views and conclusions contained in this document are those of the authors and should not be interpreted as necessarily representing the official policies, either express or implied, of the U. S. Government. The seismic and paleoearthquake data used in this article can be obtained by e-mailing a request to Robert B. Smith, rbsmith@mines.utah.edu, phone (801) 581-1729, 135 South 1460 East, Room 702, University of Utah, Salt Lake City, Utah, 84112.

References

Abrahamson, N. A., and W. J. Silva (1997). Empirical response spectral attenuation relations for shallow crustal earthquakes, *Seism. Res. Lett.* **68,** 9–23.

Arabasz, W. J., J. C. Pechmann, and E. D. Brown (1992). Observational seismology and the evaluation of earthquake hazards and risk in the Wasatch Front area, Utah, in *Assessment of Regional Earthquake Hazards and Risk Along the Wasatch Front, Utah*, P. L. Gori and W. W. Hays (Editors), *U.S. Geol. Surv. Profess. Pap. 1500-A-J*, D1–D36.

Barrientos, S. E., R. S. Stein, and S. N. Ward (1987). Comparison of the 1959 Hebgen Lake, Montana and the 1983 Borah Peak, Idaho, earthquakes from geodetic observations, *Bull. Seism. Soc. Am.* **77,** 784–808.

Black, B. D., S. Hecker, J. L. Jarva, M. D. Hylland, and G. E. Christenson (2000). *Quaternary Fault and Fold Database and Map of Utah*, unpublished Final Technical Report to the U.S. Geol. Surv., Utah Geol. Surv., scale 1:500,000.

Bruhn, R. L., and R. A. Schultz (1996). Geometry and slip distribution in normal fault system: implication for mechanics and fault-related hazards, *J. Geophys. Res.* **101,** 3401–3412.

Brune, J. N. (1979). Implications of earthquake triggering and rupture propagation for earthquake prediction based on premonitory phenomena, *J. Geophys. Res.* **84,** 2195–2198.

Campbell, K. C. (1997). Empirical near-source attenuation relationships for horizontal and vertical components of peak ground acceleration, peak ground velocity, and pseudo-absolute acceleration response spectra, *Seism. Res. Lett.* **68,** 154–179.

Caskey, S. J., and S. G. Wesnousky (1997). Static stress changes and earthquake triggering during the 1954 Fairview Peak and Dixie Valley earthquakes, Central Nevada, *Bull. Seism. Soc. Am.* **87,** 521–527.

Chang, W. L. (1998). Earthquake hazards on the Wasatch fault: tectonically induced flooding and stress triggering of earthquakes, *M.S. Thesis*, Department of Geology and Geophysics, University of Utah, Salt Lake City, Utah, 123 pp.

Chang, W. L., C. M. Meertens, R. B. Smith, R. A. Harris, and P. Cervelli (2000). Crustal deformation and fault modeling on the Wasatch Front, Utah, from continuous and campaign GPS measurements, *EOS* **81,** F1230.

Chen, G. J. (1988). A study of seismicity and spectral source characteristics of small earthquakes: Hansel Valley, Utah, and Pocatello Valley,

Idaho, areas, *Master's Thesis*, University of Utah, Salt Lake City, Utah, 119 pp.

Cornell, C. A., and E. H. Van Marke (1969). The major influence on seismic risk, in *Proceedings Third World Conference on Earthquake Engineering*, Santiago, Chile, A-1, 69–93.

Cornell, C. A., S.-C. Wu, S. R. Winterstein, J. H. Dieterich, and R. W. Simpson (1993). Seismic hazard induced by mechanically interactive fault segments, *Bull. Seism. Soc. Am.* **83,** 436–449.

Crone, A. J., M. N. Machette, M. G. Bonilla, J. J. Lienkaemper, K. L. Pierce, W. E. Scott, and R. C. Bucknam (1987). Surface faulting accompanying the Borah Peak earthquake and segmentation of the Lost River fault, central Idaho, *Bull. Seism. Soc. Am.* **77,** 739–770.

dePolo, C. M. (1994). The maximum background earthquake for the Basin and Range province, western North America, *Bull. Seism. Soc. Am.* **84,** 466–472.

Dieterich, J. (1994). A constitutive law for rate of earthquake production and its application to earthquake clustering, *J. Geophys. Res.* **99,** 2601–2618.

Dieterich, J. H., and B. Kilgore (1996). Implications of fault constitutive properties for earthquake prediction, *Proc. Natl. Acad. Sci. U.S.A.* **93,** 3787–3794.

Doser, D. I. (1985). Source parameters and faulting processes of the 1959 Hebgen Lake, Montana, earthquake sequence, *J. Geophys. Res.* **90,** 4537–4555.

Doser, D. I. (1989). Extensional tectonics in northern Utah-southern Idaho, U.S.A., and the 1934 Hansel Valley sequence, *Phys. Earth Planet. Interiors* **54,** 120–134.

Doser, D. I., and R. B. Smith (1985). Source parameters of the 28 October 1983 Borah Peak, Idaho, earthquake from body wave analysis, *Bull. Seism. Soc. Am.* **75,** 1041–1051.

Doser, D. I., and R. B. Smith (1989). An assessment of source parameters of earthquakes in the cordillera of the western United States, *Bull. Seism. Soc. Am.* **79,** 1383–1409.

Eddington, P. K., R. B. Smith, and C. Renggli (1987). Kinematics of Basin and Range intraplate extension, in *Continental Extensional Tectonics*, M. P. Coward, J. F. Dewey, and P. L. Hancock (Editors), Spec. Pub. Geol. Soc. Lond. 28, Blackwell, Oxford, 371–392.

Frankel, A., C. Mueller, T. Barnhard, D. Perkins, E. V. Leyendecker, N. Dickman, S. Hanson, and M. Hopper (1996). *National Seismic Hazard Maps.* documentation June 1996, *U.S. Geol. Surv. Open-File Rept.* 96–532, 110 pp.

Gomberg, J., M. L. Blanpied, and N. M. Beeler (1997). Transient triggering of near and distant earthquakes, *Bull. Seism. Soc. Am.* **87,** 294–309.

Hardebeck, J. L., J. J. Nazareth, and E. Hauksson (1998). The static stress change triggering model: constraints from two southern California aftershock sequences, *J. Geophys. Res.* **103,** 24,427–24,437.

Harris, R. A. (1998). Introduction to special section: stress triggers, stress shadows, and implications for seismic hazard, *J. Geophys. Res.* **103,** 24,347–24,358.

Harris, R. A., and R. W. Simpson (1998). Suppression of large earthquakes by stress shadows: a comparison of Coulomb and rate-and state failure, *J. Geophys. Res.* **103,** 24,439–24,451.

Hecker, S. (1993). Quaternary tectonics of Utah with emphasis on earthquake-hazard characterization, Utah Geol. Surv. Bull. 127, 157 pp, 2 plates.

Hodgkinson, K. M., R. S. Stein, and G. C. P. King (1996). The 1954 Rainbow Mountain–Fairview Peak–Dixie Valley earthquakes: a triggered normal faulting sequence, *Bull. Seism. Soc. Am.* **101,** 25,459–25,471.

Hylland, M. D. (2001). Quaternary fault and fold database and map of Utah, *Program with Abstracts; Geological Hazards in Utah: Practical Information for Geologists and Engineers,* American Society of Civil Engineers, 12–16.

Jackson, M. (1991). The number and timing of Holocene paleoseismic events on the Nephi and Levan segments, Wasatch fault zone, Utah, Utah Geol. Min. Surv. Spec. Stud. 78, 23 pp.

King, G. C. P., and J. Nábelek (1985). Role of fault bends in the initial and termination of earthquake rupture, *Science* **228,** 984–987.

King, G. C. P., R. S. Stein, and J. Lin (1994). Static stress changes and the triggering of earthquakes, *Bull. Seism. Soc. Am.* **84,** 935–953.

Kostrov, B. V. (1974). Seismic moment and energy of earthquakes, and seismic flow of rock, *Izv. Acad. Sci. USSP. Phys. Solid Earth* **1,** 23–40.

Lavier, L. L., W. R. Buck, and A. N. B. Poliakov (2000). Factors controlling normal fault offset in an ideal brittle layer, *J. Geophys. Res.* **105,** 23,431–23,442.

Lund, W. R., D. P. Schwartz, W. E. Mulvey, K. E. Budding, and B. D. Black (1991). Fault behavior and earthquake recurrence on the Provo segment of the Wasatch fault zone at Mapleton, Utah County, Utah, in *Paleoseismology of Utah, Volume 1*, W. R. Lund (Editor), Utah Geol. Min. Surv. Spec. Stud. 75, 1–41.

Machette, M. N., S. F. Personius, and A. R. Nelson (1992). Paleoseismology of the Wasatch fault zone: a summary of recent investigations, interpretations, and conclusions, in *Assessment of Regional Earthquake Hazards and Risk Along the Wasatch Front, Utah*, P. L. Gori and W. W. Hays (Editors), *U.S. Geol. Surv. Prof. Pap.* 1500-A-J, A1–A71.

Martinez, L., C. M. Meertens, and R. B. Smith (1998). Rapid deformation rates along the Wasatch fault zone, Utah, from first GPS measurements with implications for earthquake hazard, *Geophys. Res. Lett.* **25,** 567–570.

Mason, D. B. (1996). Earthquake magnitude potential of the Intermountain seismic belt, USA, from surface-parameter scaling of late Quaternary faults, *Bull. Seism. Soc. Am.* **86,** 1487–1506.

McCalpin, J. P., and C. V. Nelson (2001). Paleoearthquake chronology of the SLC segment of the Wasatch fault since 15 ka, and probability of the "big one" in the next 100 years, *Program with Abstracts: Geological Hazards in Utah: Practical Information for Geologists and Engineers, ASCE*, 17–18.

McCalpin, J. P., and S. P. Nishenko (1996). Holocene paleoseismicity, temporal clustering, and probabilities of future large ($M > 7$) earthquakes on the Wasatch fault zone, Utah, *J. Geophys. Res.* **101,** 6233–6253.

McCalpin, J. P., S. L. Forman, and M. Lowe (1994). Reevaluation of Holocene faulting at the Kaysville site, Weber segment of the Wasatch fault zone, Utah, *Tectonics* **13,** 1–16.

Meertens, C. M., R. B. Smith, and C. M. Puskas (2000). Crustal deformation of the Yellowstone Caldera from campaign and continuous GPS surveys, *EOS* **81,** F1388.

Nishenko, S. P., and R. Buland (1987). A generic recurrence interval distribution for earthquake forecasting, *Bull. Seism. Soc. Am.* **77,** 1382–1399.

Olig, S. S. (1994). Seismic hazard evaluation—Kennecott tailings impoundment modernization project, Magna, Utah, in unpublished report, Woodward-Clyde Consultants, C1–C6.

Ostenaa, D. A. (1990). Late Holocene displacement history, Water Canyon site, Wasatch fault, Utah, Geol, Soc. Am. Abstr. Prog. **22,** 42.

Pechmann, J. C., and W. J. Arabasz (1995). The problem of the random earthquake in seismic hazard analysis: Wasatch Front region, Utah, in *Environmental and Engineering Geology of the Wasatch Front Region: 1995 Symposium and Field Conference*, W. R. Lund (Editor), Utah Geol. Assoc., 77–93.

Personius, S. F. (1991). Paleoseismic analysis of the Wasatch fault zone at the Brigham City trench site, Brigham City, Utah and Pole Patch trench site, Pleasant View, Utah, W. R. Lund (Editor), Utah Geol. Min. Surv. Spec. Stud. 76, 39 pp.

Pezzopane, S. K., and Dawson T. E. (1996). Fault displacement hazard: a summary of issues and information, *U.S. Geol. Surv. Yucca Mountain Report to the U.S. Department of Energy: Seismotectonic Framework and Characterization of Faulting at Yucca Mountain, Nevada, Chapter 9*, 160 pp.

Pollitz, F. F., and I. S. Sacks (1997). The 1995 Kobe, Japan, earthquake: a long-delayed aftershock of the offshore 1944 Tonankai and 1946 Nankaido earthquakes, *Bull. Seism. Soc. Am.* **87,** 1–10.

Reasenberg, P. A., and R. W. Simpson (1992). Response of regional seismicity to the static stress change produced by the Loma Prieta earthquake, *Science* **255,** 1687–1690.

Richins, W. D., J. C. Pechmann, R. B. Smith, C. J. Langer, S. K. Goter, J. E. Zollweg, and J. J. King (1987). The 1983 Borah Peak, Idaho, earthquake and its aftershocks, *Bull. Seism. Soc. Am.* **77,** 694–723.

Schwartz, D. P., and K. J. Coppersmith (1984). Fault behavior and characteristic earthquakes: examples from the Wasatch and San Andreas fault zone, *J. Geophys. Res.* **89,** 5681–5698.

Simpson, R. W., and P. A. Reasenberg (1994). Earthquake-induced static-stress changes on central California faults, *in The Loma Prieta, California, Earthquake of October 17, 1989—Tectonic Processes and Models*, R. W. Simpson (Editor), *U.S. Geol. Surv. Profess. Pap.* 1550-F, F55–F89.

Smith, R. B., and W. J. Arabasz (1991). Seismicity of the Intermountain Seismic Belt, in *Neotectonics of North America*, D. B. Slemmons, E. R. Engdahl, M. L. Zoback, and D. D. Blackwell (Editors), Geol. Soc. Am., SMV V-1, Decade Map 1, 185–228.

Smith, R. B., and R. L. Bruhn (1984). Intraplate extensional tectonics of the eastern Basin-Range: inferences on structural style from seismic reflection data, regional tectonics, and thermal-mechanical models of brittle-ductile deformation, *J. Geophys. Res.* **89,** 5733–5762.

Smith, R. B., and M. L. Sbar (1974). Contemporary tectonic and seismicity of the western United States with emphasis on the Intermountain Seismic Belt, *Bull. Geol. Soc. Am.* **85,** 1205–1218.

Spudich, P., J. Fletcher, M. Hellweg, J. Boatwright, C. Sullivan, W. B. Joyner, T. C. Hanks, D. M. Boore, A. F. McGarr, L. M. Baker, and A. G. Lindh (1997). SEA96: a new predictive relation for earthquake ground motions in extensional tectonic regimes, *Seism. Res. Lett.* **68,** 190–198.

Spudich, P. J., W. B. Joyner, A. G. Lindh, D. M. Boore, B. M. Margaris, and J. B. Fletcher (1999). SEA99: a revised ground motion prediction relation for use in extensional tectonic regimes, *Bull. Seism. Soc. Am.* **89,** 1156–1170.

Stein, R. S., A. A. Barka, and J. H. Dieterich (1997). Progressive failure on the North Anatolian fault since 1939 by earthquake stress triggering, *Geophys. J. Int.* **128,** 594–604.

Swan, F. H. III, D. P. Schwartz, and L. S. Cluff (1980). Recurrence of moderate to large magnitude earthquakes produced by surface faulting on the Wasatch fault, Utah, *Bull. Seism. Soc. Am.* **70,** 1431–1462.

Toda, S., R. S. Stein, P. A. Reasenberg, J. H. Dieterich, and A. Yoshida (1998). Stress transferred by the 1995 $M_w = 6.9$ Kobe, Japan, shock: effect on aftershocks and future earthquake probabilities, *J. Geophys. Res.* **103,** 24,543–24,567.

Waite, G. P., and R. B. Smith (2000). Seismicity of the Yellowstone volcanic field: regional stress inversion and analysis of the autumn 1985 Earthquake Swarm, *EOS* **80,** F1388.

Ward, S. N. (1998). On the consistency of earthquake moment rates, geological fault data, and space geodetic strain: the United States, *Geophys. J. Int.* **134,** 172–186.

Wells, D. L., and K. J. Coppersmith (1994). New empirical relationships among magnitude, rupture length, rupture width, rupture area, and surface displacement, *Bull. Seism. Soc. Am.* **84,** 974–1002.

Wesnousky, S. G. (1994). The Gutenberg–Richard or characteristic earthquake distribution, which is it?, *Bull. Seism. Soc. Am.* **84,** 1940–1959.

Wesnousky, S. G., C. H. Scholtz, K. Shimazaki, and T. Matsuda (1984). Earthquake frequency distribution and the mechanics of faulting, *J. Geophys. Res.* **88,** 9331–9340.

Wheeler, R. L., and K. B. Krystinik (1992). Persistent and nonpersistent segmentation of the Wasatch Fault Zone, Utah: statistical analysis for evaluation of seismic hazard, in *Assessment of Regional Earthquake Hazards and Risk Along the Wasatch Front, Utah*, P. L. Gori and W. W. Hays (Editors), *U.S. Geol. Surv. Profess. Pap.* 1500-A-J, B1–B47.

Wiemer, S. (1996). *ZMAP User Guide*, Univ. of Alaska at Fairbanks, 115 pp.

Wong, I. G., S. S. Olig, R. Green, Y. Moriwaki, N. Abrahamson, D. Baures, W. Silva, P. Somerville, D. Davidson, J. Pilz, and B. Dunne (1995). Seismic hazard evaluation of the Magna tailings impoundment, in *Environmental and Engineering Geology of the Wasatch Front Region*, W. R. Lund (Editor), Utah Geol. Assoc., 95–110.

Wong, I. G., W. Silva, S. Olig, P. Thomas, D. Wright, F. Ashland, N. Gregor, J. Pechmann, M. Dober, and G. Christenson (2001). Microzonation maps for earthquake ground shaking in Salt Lake City metropolitan area, Utah, Program with Abstracts: Geological Hazards In Utah: Practical Information for Geologists and Engineers, ASCE, 5–6.

Working Group on California Earthquake Probabilities (1995). Seismic hazards in southern California: probable earthquakes, 1994 to 2024, *Bull. Seism. Soc. Am.* **85,** 379–439.

Youngs, R. R., and K. J. Coppersmith (1985). Implications of fault slip rates and earthquake recurrence models to probabilistic seismic hazard estimates, *Bull. Seism. Soc. Am.* **75,** 939–964.

Youngs, R. R., F. H. Swan, M. S. Power, D. P. Schwartz, and R. K. Green (1987). Probabilistic analysis of earthquake ground shaking hazard along the Wasatach Front, Utah, in *Assessment of Regional Earthquake Hazards and Risk Along the Wasatch Front, Utah*, P. L. Gori and W. W. Hays (Editors), *U.S. Geol. Surv. Open-File Rept.* 87-585, M1–M110.

Zoback, M. L. (1989). State of stress and modern deformation of the northern Basin and Range province, *J. Geophys. Res.* **94,** 7105–7128.

Appendix

Earthquake Source and Recurrence Model for the Wasatch Fault Zone

Source Type	Name of Fault or Fault Segment	Recurrence Model
Type A	BC, WB, SLC, PV, NP (Wasatch Fault)	Characteristic model (from paleoseismic data): Lognormal distribution ($\sigma_D = 0.21$ or 0.5)
Type B	LV (Wasatch Fault), EC, HV, NO, SB, MC, EGSL, EBL, BR, RC	Characteristic model (from fault slip rate)*. $\dot{M}_{seismic} = \mu LWV$; $M(m_u) = 10^{1.5m+9}$; $N_B = \frac{\dot{M}_{seismic}}{M(m_u)}$
Type C	Background seismicity	Truncated-exponential model:† $N_C(m) = 10^{a-b(m-m_0)} - n(m_u)$; $C_d(m_1, m_2) = \frac{\int_{m_1}^{m_2} 10^{a-bm} \cdot 10^{1.5m+9} dm}{\int_{m_1}^{m_2} 10^{a-bm} dm}$
		Historical seismicity: $N_C(m) = 3.2 \times 10^{-0.72(m-3.0)} - 1.2 \times 10^{-3}$
		Geological moment rate: $\dot{M}_{seismic} = \mu LWV$; $N_C(6.6) = \frac{\dot{M}_{seismic}}{C_d(6.6, m_u)}$, $b = 0.76$
		Geodetic (GPS) moment rate: $\dot{M}_{seismic} = 2\mu HLW\,\dot{\varepsilon} - \mu LWV$; $N_C(3.0) = \frac{\dot{M}_{seismic}}{C_d(3.0, m_u)}$, $b = 0.76$

*$\dot{M}_{seismic}$, *seismic-moment rate;* $M(m)$, seismic moment of magnitude m; μ, rigidity. For each fault: L, fault length; W, fault width; V, slip rate; m_u, maximum magnitude; N_B, annual frequency of characteristic earthquakes on type B faults.
†$N_c(m)$, annual frequency of type C source with magnitude m; $\dot{\varepsilon}$, strain rate; H, elastic depth of the crust (15 km for this study).

Department of Geology and Geophysics
University of Utah,
Salt Lake City, Utah
(W.-L.C., R.B.S.)

Manuscript received 31 May 2001.